

# Pair size and quantum geometry in a multiband Hubbard model

M. Iskin

*Department of Physics, Koç University, Rumelifeneri Yolu, 34450 Sarıyer, İstanbul, Türkiye*

(Dated: December 24, 2024)

We study the size of two-body bound states and Cooper pairs within a multiband Hubbard model that features time-reversal symmetry and uniform pairing on a generic lattice. Our analysis involves (i) an exact calculation of the localization tensor to determine the size of lowest-lying two-body bound state in vacuum, and (ii) an evaluation of the analogous tensor to estimate the average size of Cooper pairs within the mean-field BCS-BEC crossover theory at zero temperature. Beyond the conventional intraband contribution that depends on Bloch bands, we show that pair size also has a geometric contribution governed by the quantum-metric tensor of the Bloch states and their band-resolved quantum-metric tensors. As a concrete example, we investigate the pyrochlore-Hubbard model numerically and demonstrate that, while the pair size diverges in the weakly interacting BCS regime of dispersive bands, it remains finite and relatively small in the flat-band regime, even for infinitesimal interaction, perfectly matching the exact two-body result in the dilute limit.

## I. INTRODUCTION

The quantum geometry of a Bloch band is characterized by the quantum-metric tensor, which corresponds to the real part of the quantum-geometric tensor and measures the so-called quantum distance between two nearby Bloch states [1, 2]. Recent studies on multiband Hubbard models have revealed that this band invariant plays a crucial role in describing virtual interband processes that influence key observables in superconductivity. These include, but are not limited to, the superfluid weight, superfluid density, critical transition temperature, low-energy collective excitations, and the Ginzburg-Landau (GL) coherence length [3–16]. The quantum geometry inherent in multiband systems modifies these observables, demonstrating that the quantum metric is not merely a mathematical artifact but a central quantity in determining the physical behavior of superconductors, particularly in flat-band systems where geometric effects are more pronounced. It is important to emphasize that these observables are not independent but are instead directly linked through the effective-mass tensor of Cooper pairs [6, 17]. This connection is also rooted in the effective-mass tensor of the lowest-lying two-body bound states in vacuum [3, 18]. For this reason, the geometric nature of superconducting pairing manifests itself across multiple physical quantities, showing that the quantum metric is an essential component of the underlying physics in multiband superconductors.

In this study, we investigate the role of quantum geometry in determining the size of two-body bound states and Cooper pairs within a generic multiband Hubbard model that exhibits time-reversal symmetry and uniform pairing. We analyze the localization tensors for the lowest-lying two-body bound state in vacuum and the average size of Cooper pairs within the mean-field BCS-BEC crossover theory at zero temperature. Our main result highlights a stark contrast between the BCS regime of dispersive bands and the flat-band regime: while the pair size diverges in the weakly interacting BCS regime, it remains finite and relatively small in the flat-band regime,

even for infinitesimal interactions, where it is governed entirely by the quantum metric. It is pleasing to note that this result is consistent with the modern theory of insulating states, where the localization tensor diverges in the thermodynamic limit for metals, while it remains finite for insulators [1]. We also emphasize that pair size and coherence length, though related, are distinct physical quantities with different quantum-geometric origins. The coherence length is linked to the motion of Cooper pairs via the inverse effective-mass tensor [8, 9, 14], whereas the pair size does not have a direct relationship with the effective mass or center-of-mass momentum of the pair, distinguishing it from previous studies in this context. Away from the flat-band regime, the pair size mirrors the zero-temperature coherence length [14], scaling inversely with the order parameter across much of the parameter space. However, in stark contrast to the finite and relatively small pair size in the dilute flat-band regime, the coherence length has recently been shown to diverge in this limit [14].

The remaining text is organized as follows. In Sec. II, we introduce the multiband Hubbard model in reciprocal space. In Sec. III, we derive the size of two-body bound states in vacuum through an exact calculation of the localization tensor. In Sec. IV, we estimate the average size of Cooper pairs within the mean-field BCS-BEC crossover theory at zero temperature. In Sec. V, we present the numerical calculations for the pyrochlore-Hubbard model. The paper concludes with a summary in Sec. VI, and an alternative but failed approach to the size of Cooper pairs is discussed in the Appendix.

## II. MULTIBAND HUBBARD MODEL

The multiband Hubbard model  $\mathcal{H} = \sum_{\sigma} \mathcal{H}_{\sigma} + \mathcal{H}_{\uparrow\downarrow}$  consists of two parts. The non-interacting part  $\mathcal{H}_{\sigma} = -\sum_{i i' S S'} t_{i S; i' S'}^{\sigma} c_{S i' \sigma}^{\dagger} c_{S i \sigma}$  describes the hopping processes between lattice sites, where the operator  $c_{S i \sigma}^{\dagger}$  creates a spin- $\sigma$  fermion on the sublattice site  $S$  in the  $i$ th

unit cell, and  $t_{iS;i'S'}^\sigma$  is the hopping parameter between site  $S'$  in unit cell  $i'$  and site  $S$  in unit cell  $i$ . To reexpress  $\mathcal{H}_\sigma$  in reciprocal space, we introduce a canonical transformation,  $c_{Si\sigma}^\dagger = \frac{1}{\sqrt{N_c}} \sum_{\mathbf{k}} e^{-i\mathbf{k}\cdot\mathbf{r}_{iS}} c_{S\mathbf{k}\sigma}^\dagger$ , where  $N_c$  is the number of unit cells in the system,  $\mathbf{k} = (k_x, k_y, k_z)$  is the crystal momentum (in units of  $\hbar \rightarrow 1$ ) within the first Brillouin zone (BZ), and  $\mathbf{r}_{iS}$  is the position of site  $S \in i$ . The momentum summation satisfies  $\sum_{\mathbf{k} \in \text{BZ}} 1 = N_c$ , and when the number of sublattice sites within a unit cell is  $N_b$ , the total number of lattice sites in the system is  $N = N_b N_c$ . This transformation leads to the Bloch Hamiltonian in the sublattice basis,

$$\mathcal{H}_\sigma = \sum_{SS'\mathbf{k}} h_{SS'\mathbf{k}}^\sigma c_{S\mathbf{k}\sigma}^\dagger c_{S'\mathbf{k}\sigma}, \quad (1)$$

where the matrix elements  $h_{SS'\mathbf{k}}^\sigma = -\frac{1}{N_c} \sum_{ii'} t_{iS;i'S'}^\sigma e^{i\mathbf{k}\cdot(\mathbf{r}_{iS}-\mathbf{r}_{i'S'})}$  determine the single-particle spectrum via the eigenvalue relation

$$\sum_{S'} h_{SS'\mathbf{k}}^\sigma n_{S'\mathbf{k}\sigma} = \varepsilon_{n\mathbf{k}\sigma} n_{S\mathbf{k}\sigma}. \quad (2)$$

Here,  $\varepsilon_{n\mathbf{k}\sigma}$  represents the energy of the  $n$ th Bloch band, and  $n_{S\mathbf{k}\sigma}$  is the periodic part of the corresponding Bloch wave function, as discussed further below. Finally, applying the basis transformation  $c_{S\mathbf{k}\sigma}^\dagger = \sum_n n_{S\mathbf{k}\sigma}^* c_{n\mathbf{k}\sigma}^\dagger$ , we recast the Hamiltonian in the band basis as  $\mathcal{H}_\sigma = \sum_{n\mathbf{k}} \varepsilon_{n\mathbf{k}\sigma} c_{n\mathbf{k}\sigma}^\dagger c_{n\mathbf{k}\sigma}$ . On the other hand, the interacting part  $\mathcal{H}_{\uparrow\downarrow} = -U \sum_{iS} c_{Si\uparrow}^\dagger c_{Si\downarrow}^\dagger c_{Si\downarrow} c_{Si\uparrow}$  with  $U \geq 0$  describes the on-site density-density attraction between spin- $\uparrow$  and spin- $\downarrow$  fermions. In reciprocal space, we re-express it as

$$\mathcal{H}_{\uparrow\downarrow} = -\frac{U}{N_c} \sum_{S\mathbf{k}\mathbf{k}'\mathbf{q}} c_{S,\mathbf{k}+\frac{\mathbf{q}}{2}\uparrow}^\dagger c_{S,-\mathbf{k}+\frac{\mathbf{q}}{2}\downarrow}^\dagger c_{S,-\mathbf{k}'+\frac{\mathbf{q}}{2}\downarrow} c_{S,\mathbf{k}'+\frac{\mathbf{q}}{2}\uparrow}. \quad (3)$$

Next, we take advantage of the explicit conservation of total momentum in the  $\mathbf{k}$ -space formulation and present an exact solution for the two-body problem.

### III. EXACT TWO-BODY PROBLEM

To solve for the spin-singlet bound states of a pair of spin- $\uparrow$  and spin- $\downarrow$  fermions with center-of-mass momentum  $\mathbf{q}$ , we adopt the ansatz state [18]

$$|\Psi_{\mathbf{q}}\rangle = \sum_{n\mathbf{m}\mathbf{k}} \alpha_{n\mathbf{m}\mathbf{k}}^{\mathbf{q}} c_{n,\mathbf{k}+\frac{\mathbf{q}}{2}\uparrow}^\dagger c_{m,-\mathbf{k}+\frac{\mathbf{q}}{2}\downarrow}^\dagger |0\rangle, \quad (4)$$

where  $|0\rangle$  is the vacuum state, and  $\alpha_{n\mathbf{m}\mathbf{k}}^{\mathbf{q}}$  are the variational parameters. The requirement  $\alpha_{n\mathbf{m}\mathbf{k}}^{\mathbf{q}} = \alpha_{m\mathbf{n},-\mathbf{k}}^{\mathbf{q}}$  ensures that  $|\Psi_{\mathbf{q}}\rangle$  is antisymmetric under the exchange of fermions, which is necessary and sufficient for the spin-singlet state. The normalization condition  $\langle \Psi_{\mathbf{q}} | \Psi_{\mathbf{q}} \rangle = 1$  leads to the constraint  $\sum_{n\mathbf{m}\mathbf{k}} |\alpha_{n\mathbf{m}\mathbf{k}}^{\mathbf{q}}|^2 = 1$ . For any given

$\mathbf{q}$ , minimization of the expectation value  $\langle \Psi_{\mathbf{q}} | \mathcal{H} - E_{\mathbf{q}} | \Psi_{\mathbf{q}} \rangle$  with respect to  $\alpha_{n\mathbf{m}\mathbf{k}}^{\mathbf{q}}$ , where  $E_{\mathbf{q}}$  represents the energy of the allowed two-body states, leads to a set of linear equations [18]

$$\alpha_{n\mathbf{m}\mathbf{k}}^{\mathbf{q}} = \frac{U \sum_S \beta_{S\mathbf{q}} n_{S,\mathbf{k}+\frac{\mathbf{q}}{2}\uparrow}^* m_{S,-\mathbf{k}+\frac{\mathbf{q}}{2}\downarrow}^*}{\varepsilon_{n,\mathbf{k}+\frac{\mathbf{q}}{2}\uparrow} + \varepsilon_{m,-\mathbf{k}+\frac{\mathbf{q}}{2}\downarrow} - E_{\mathbf{q}}}. \quad (5)$$

Here, the dressed variational parameters  $\beta_{S\mathbf{q}} = \sum_{n\mathbf{m}\mathbf{k}} \alpha_{n\mathbf{m}\mathbf{k}}^{\mathbf{q}} n_{S,\mathbf{k}+\frac{\mathbf{q}}{2}\uparrow} m_{S,-\mathbf{k}+\frac{\mathbf{q}}{2}\downarrow}$  characterize the physical properties of the two-body bound states, and  $E_{\mathbf{q}}$  are given by the eigenvalues of an  $N_b^2 N_c \times N_b^2 N_c$  matrix through Eq. (5). Next, we discuss the two-body wave function and its localization tensor from which the pair size follows.

#### A. Localization tensor for the bound states

The wave function for the resultant two-body bound states is determined by  $\Psi_{\mathbf{q}}(\mathbf{r}_1, \mathbf{r}_2) = \langle \mathbf{r}_1 \mathbf{r}_2 | \Psi_{\mathbf{q}} \rangle$ , where  $\mathbf{r}_1 = (x_1, y_1, z_1)$  and  $\mathbf{r}_2 = (x_2, y_2, z_2)$  are the Cartesian components. Here, we express the Bloch wave function for a spin- $\sigma$  particle as  $\phi_{n\mathbf{k}\sigma}(\mathbf{r}) = \langle \mathbf{r} | n\mathbf{k}\sigma \rangle = \frac{e^{i\mathbf{k}\cdot\mathbf{r}}}{\sqrt{N_c}} n_{\mathbf{k}\sigma}(\mathbf{r})$ , where  $|n\mathbf{k}\sigma\rangle = c_{n\mathbf{k}\sigma}^\dagger |0\rangle$  and  $n_{\mathbf{k}\sigma}(\mathbf{r})$  represents the periodic part of the wave function. This leads to  $\Psi_{\mathbf{q}}(\mathbf{r}_1, \mathbf{r}_2) = \frac{e^{i\mathbf{q}\cdot\mathbf{R}}}{N_c} \sum_{n\mathbf{m}\mathbf{k}} e^{i\mathbf{k}\cdot\mathbf{r}} \alpha_{n\mathbf{m}\mathbf{k}}^{\mathbf{q}} n_{\mathbf{k}+\frac{\mathbf{q}}{2}\uparrow}(\mathbf{r}_1) m_{-\mathbf{k}+\frac{\mathbf{q}}{2}\downarrow}(\mathbf{r}_2)$ , where  $\mathbf{R} = (\mathbf{r}_1 + \mathbf{r}_2)/2$  is the center-of-mass position of the pair, and  $\mathbf{r} = \mathbf{r}_1 - \mathbf{r}_2$  is the relative position of its constituents. Note that  $\Psi_{\mathbf{q}}(\mathbf{r}_1, \mathbf{r}_2) = \Psi_{\mathbf{q}}(\mathbf{r}_2, \mathbf{r}_1)$  upon spin exchange by construction when  $\uparrow \leftrightarrow \downarrow$ . For the multiband Hubbard model of interest in this paper, we substitute  $\mathbf{r}_1 \rightarrow \mathbf{r}_{iS}$  and  $\mathbf{r}_2 \rightarrow \mathbf{r}_{i'S'}$ , leading to  $\Psi_{\mathbf{q}}(\mathbf{r}_{iS}, \mathbf{r}_{i'S'}) = e^{i\mathbf{q}\cdot(\mathbf{r}_{iS}+\mathbf{r}_{i'S'})/2} \psi_{SS'}^{\mathbf{q}}(\bar{\mathbf{r}})$ , where  $\bar{\mathbf{r}} = \mathbf{r}_{iS} - \mathbf{r}_{i'S'}$  is the relative position. The latter function is defined as

$$\psi_{SS'}^{\mathbf{q}}(\bar{\mathbf{r}}) = \frac{1}{N_c} \sum_{n\mathbf{m}\mathbf{k}} e^{i\mathbf{k}\cdot\bar{\mathbf{r}}} \alpha_{n\mathbf{m}\mathbf{k}}^{\mathbf{q}} n_{S,\mathbf{k}+\frac{\mathbf{q}}{2}\uparrow} m_{S',-\mathbf{k}+\frac{\mathbf{q}}{2}\downarrow}, \quad (6)$$

with the constraint  $\sum_{iS i'S'} |\psi_{SS'}^{\mathbf{q}}(\bar{\mathbf{r}})|^2 = \sum_{n\mathbf{m}\mathbf{k}} |\alpha_{n\mathbf{m}\mathbf{k}}^{\mathbf{q}}|^2 = 1$ . This normalization condition follows simply from the orthonormalization conditions  $\frac{1}{N_c} \sum_i e^{i(\mathbf{k}-\mathbf{k}')\cdot\mathbf{r}_{iS}} = \delta_{\mathbf{k}\mathbf{k}'}$  and  $\sum_S n_{S\mathbf{k}\sigma}^* m_{S\mathbf{k}\sigma} = \langle n_{\mathbf{k}\sigma} | m_{\mathbf{k}\sigma} \rangle = \delta_{nm}$ , where  $\delta_{ij}$  is the Kronecker-delta.

For the simplicity of the presentation, we denote the Cartesian components of the relative position as  $\mathbf{r} = (r_x, r_y, r_z)$  where  $r_x = x_1 - x_2$ ,  $r_y = y_1 - y_2$ , and  $r_z = z_1 - z_2$ . It is easy to see that  $\langle \Psi_{\mathbf{q}} | r_i | \Psi_{\mathbf{q}} \rangle = \sum_{\mathbf{r}_1 \mathbf{r}_2} r_i |\Psi_{\mathbf{q}}(\mathbf{r}_1, \mathbf{r}_2)|^2 = 0$ , since changing the dummy summation indices  $\mathbf{r}_1 \leftrightarrow \mathbf{r}_2$  changes the overall sign of the summand. Then, to extract the pair size from the variance of the relative position, we introduce the so-called localization tensor [1], whose real and symmetric matrix elements are given by  $(\xi_{2b}^2)_{ij} = \langle \Psi_{\mathbf{q}} | r_i r_j | \Psi_{\mathbf{q}} \rangle = \sum_{\mathbf{r}_1 \mathbf{r}_2} r_i r_j |\Psi_{\mathbf{q}}(\mathbf{r}_1, \mathbf{r}_2)|^2$ . For the multiband Hubbard model

of interest in this paper, it can be written as

$$(\xi_{2b}^2)_{ij} = \sum_{iS'i'S'} \bar{r}_i \bar{r}_j |\psi_{SS'}^{\mathbf{q}}(\bar{\mathbf{r}})|^2, \quad (7)$$

where  $\bar{r}_i$  is the  $i$ -component of  $\bar{\mathbf{r}}$ . Then, we substitute  $r_i e^{i\mathbf{k}\cdot\mathbf{r}} = -i\partial_i(e^{i\mathbf{k}\cdot\mathbf{r}})$  and  $r_j e^{-i\mathbf{k}'\cdot\mathbf{r}} = i\partial_{j'}(e^{-i\mathbf{k}'\cdot\mathbf{r}})$ , where  $\partial_i \equiv \frac{\partial}{\partial k_i}$  and  $\partial_{j'} \equiv \frac{\partial}{\partial k'_{j'}}$ , and use Green's theorem for periodic functions [19], i.e., integration by parts. This shifts the partial derivatives from the exponential factors to the Bloch factors. Summing over the unit cells through the

orthonormalization condition for the exponential factors, we eventually find

$$(\xi_{2b}^2)_{ij} = \sum_{nmn'm'S'S'\mathbf{k}} \partial_i(\alpha_{nm\mathbf{k}}^{\mathbf{q}} n_{S,\mathbf{k}+\frac{\mathbf{q}}{2},\uparrow} m_{S',-\mathbf{k}+\frac{\mathbf{q}}{2},\downarrow}) \times \partial_j(\alpha_{n'm'\mathbf{k}}^{\mathbf{q}} n'_{S,\mathbf{k}+\frac{\mathbf{q}}{2},\uparrow} m'_{S',-\mathbf{k}+\frac{\mathbf{q}}{2},\downarrow})^*. \quad (8)$$

This expression can also be reexpressed in alternative forms [20]. After performing the derivatives, it leads to a relatively complicated expression

$$\begin{aligned} (\xi_{2b}^2)_{ij} = & \sum_{nm\mathbf{k}} \partial_i \alpha_{nm\mathbf{k}}^{\mathbf{q}} \partial_j (\alpha_{nm\mathbf{k}}^{\mathbf{q}})^* + \sum_{nm\mathbf{k}} \partial_i \alpha_{nm\mathbf{k}}^{\mathbf{q}} (\alpha_{n'm'\mathbf{k}}^{\mathbf{q}})^* \left( \langle \partial_j n'_{\mathbf{k}+\frac{\mathbf{q}}{2},\uparrow} | n_{\mathbf{k}+\frac{\mathbf{q}}{2},\uparrow} \rangle \delta_{mm'} + \langle \partial_j m'_{-\mathbf{k}+\frac{\mathbf{q}}{2},\downarrow} | m_{-\mathbf{k}+\frac{\mathbf{q}}{2},\downarrow} \rangle \delta_{nn'} \right) \\ & + \sum_{nmn'm'\mathbf{k}} \alpha_{nm\mathbf{k}}^{\mathbf{q}} \partial_j (\alpha_{n'm'\mathbf{k}}^{\mathbf{q}})^* \left( \langle n'_{\mathbf{k}+\frac{\mathbf{q}}{2},\uparrow} | \partial_i n_{\mathbf{k}+\frac{\mathbf{q}}{2},\uparrow} \rangle \delta_{mm'} + \langle m'_{-\mathbf{k}+\frac{\mathbf{q}}{2},\downarrow} | \partial_i m_{-\mathbf{k}+\frac{\mathbf{q}}{2},\downarrow} \rangle \delta_{nn'} \right) \\ & + \sum_{nmn'm'\mathbf{k}} \alpha_{nm\mathbf{k}}^{\mathbf{q}} (\alpha_{n'm'\mathbf{k}}^{\mathbf{q}})^* \left( \langle \partial_j n'_{\mathbf{k}+\frac{\mathbf{q}}{2},\uparrow} | \partial_i n_{\mathbf{k}+\frac{\mathbf{q}}{2},\uparrow} \rangle \delta_{mm'} + \langle \partial_j m'_{-\mathbf{k}+\frac{\mathbf{q}}{2},\downarrow} | \partial_i m_{-\mathbf{k}+\frac{\mathbf{q}}{2},\downarrow} \rangle \delta_{nn'} \right. \\ & \left. + \langle n'_{\mathbf{k}+\frac{\mathbf{q}}{2},\uparrow} | \partial_i n_{\mathbf{k}+\frac{\mathbf{q}}{2},\uparrow} \rangle \langle \partial_j m'_{-\mathbf{k}+\frac{\mathbf{q}}{2},\downarrow} | m_{-\mathbf{k}+\frac{\mathbf{q}}{2},\downarrow} \rangle + \langle \partial_j n'_{\mathbf{k}+\frac{\mathbf{q}}{2},\uparrow} | n_{\mathbf{k}+\frac{\mathbf{q}}{2},\uparrow} \rangle \langle m'_{-\mathbf{k}+\frac{\mathbf{q}}{2},\downarrow} | \partial_i m_{-\mathbf{k}+\frac{\mathbf{q}}{2},\downarrow} \rangle \right). \quad (9) \end{aligned}$$

To make further analytical progress, we next consider a generic multiband Hubbard model that exhibits time-reversal symmetry and uniform pairing across the underlying sublattices within a unit cell, and focus on the lowest-lying bound state with  $\mathbf{q} = \mathbf{0}$ .

## B. Uniform-pairing condition

In the remaining text, we assume that the Bloch Hamiltonian manifests time-reversal symmetry, where  $h_{SS'\mathbf{k}}^\uparrow = (h_{S'S',-\mathbf{k}}^\downarrow)^*$ , which implies that  $n_{S,-\mathbf{k},\downarrow}^* = n_{S\mathbf{k}\uparrow} \equiv n_{S\mathbf{k}}$  for the Bloch factors and  $\varepsilon_{n,-\mathbf{k},\downarrow} = \varepsilon_{n\mathbf{k}\uparrow} \equiv \varepsilon_{n\mathbf{k}}$  for the Bloch bands. Furthermore, we assume that the so-called uniform-pairing condition, i.e.,  $\beta_{S\mathbf{q}} \equiv \beta_{\mathbf{q}}$  for every sublattice site  $S$  within a unit cell, is satisfied for the lowest-lying bound states  $E_{\mathbf{q}}$  in the  $\mathbf{q} \rightarrow \mathbf{0}$  limit. Under these assumptions,  $E_{\mathbf{q}}$  can be Taylor expanded as  $E_{\mathbf{q}} = E_b + \frac{1}{2} \sum_{ij} (M_{2b}^{-1})_{ij} q_i q_j + \dots$ , where  $E_b = E_{\mathbf{0}}$  is the energy offset determined by  $1 = \frac{U}{N} \sum_{n\mathbf{k}} 1/(2\varepsilon_{n\mathbf{k}} - E_b)$  and the matrix elements  $(M_{2b}^{-1})_{ij}$  constitute the inverse effective-mass tensor [18]. In addition, Eq. (5) reduces to  $\alpha_{nm\mathbf{k}}^{\mathbf{0}} = \alpha_{nm\mathbf{k}}^{\mathbf{0}} \delta_{nm}$  at  $\mathbf{q} = \mathbf{0}$ , where  $\alpha_{nm\mathbf{k}}^{\mathbf{0}} = U\beta_{\mathbf{0}}/[N_c(2\varepsilon_{n\mathbf{k}} - E_b)]$ , and the normalization condition requires  $(\frac{N_c}{U|\beta_{\mathbf{0}}|})^2 = \sum_{n\mathbf{k}} \frac{1}{(2\varepsilon_{n\mathbf{k}} - E_b)^2}$ . Noting that  $\alpha_{nm\mathbf{k}}^{\mathbf{0}} (\alpha_{m\mathbf{k}}^{\mathbf{0}})^*$  is a real number and using  $\langle \partial_i n_{\mathbf{k}\sigma} | m_{\mathbf{k}\sigma} \rangle = -\langle n_{\mathbf{k}\sigma} | \partial_i m_{\mathbf{k}\sigma} \rangle$  in Eq. (9), we can express the localization tensor as  $(\xi_{2b}^2)_{ij} = (\xi_{2b}^2)_{ij}^{\text{intra}} + (\xi_{2b}^2)_{ij}^{\text{inter}}$ , where  $(\xi_{2b}^2)_{ij}^{\text{intra}} = \sum_{n\mathbf{k}} \partial_i \alpha_{nm\mathbf{k}}^{\mathbf{0}} \partial_j (\alpha_{nm\mathbf{k}}^{\mathbf{0}})^*$  is the intra-band contribution and  $(\xi_{2b}^2)_{ij}^{\text{inter}} = \sum_{n\mathbf{k}} |\alpha_{nm\mathbf{k}}^{\mathbf{0}}|^2 g_{ij}^{n\mathbf{k}} -$

$\sum_{n,m \neq n,\mathbf{k}} \alpha_{nm\mathbf{k}}^{\mathbf{0}} (\alpha_{m\mathbf{k}}^{\mathbf{0}})^* g_{ij}^{n\mathbf{k}}$  is the interband contribution. Here,  $g_{ij}^{n\mathbf{k}} = \sum_{m \neq n} g_{ij}^{m\mathbf{k}}$  is the quantum-metric tensor of the  $n$ th Bloch band, where

$$g_{ij}^{n\mathbf{k}} = 2\text{Re} \langle \partial_i n_{\mathbf{k}} | m_{\mathbf{k}} \rangle \langle m_{\mathbf{k}} | \partial_j n_{\mathbf{k}} \rangle \quad (10)$$

is the so-called band-resolved quantum-metric tensor, with Re denoting the real part. Note that while  $g_{ij}^{n\mathbf{k}} = g_{ji}^{n\mathbf{k}}$  is symmetric,  $g_{ij}^{n\mathbf{k}} = g_{ji}^{m\mathbf{k}}$  is not. More explicitly, the alternative expressions

$$\begin{aligned} (\xi_{2b}^2)_{ij}^{\text{intra}} &= \frac{4 \sum_{n\mathbf{k}} \frac{\partial_i \varepsilon_{n\mathbf{k}} \partial_j \varepsilon_{n\mathbf{k}}}{(2\varepsilon_{n\mathbf{k}} - E_b)^4}}{\sum_{n\mathbf{k}} \frac{1}{(2\varepsilon_{n\mathbf{k}} - E_b)^2}}, \quad (11) \\ (\xi_{2b}^2)_{ij}^{\text{inter}} &= \frac{\sum_{n\mathbf{k}} \frac{g_{ij}^{n\mathbf{k}}}{(2\varepsilon_{n\mathbf{k}} - E_b)^2} - \sum_{n,m \neq n,\mathbf{k}} \frac{g_{ij}^{n\mathbf{k}}}{(2\varepsilon_{n\mathbf{k}} - E_b)(2\varepsilon_{m\mathbf{k}} - E_b)}}{\sum_{n\mathbf{k}} \frac{1}{(2\varepsilon_{n\mathbf{k}} - E_b)^2}}, \quad (12) \end{aligned}$$

offer a direct term-by-term comparison with the previous results on the inverse effective-mass tensor  $(M_{2b}^{-1})_{ij}$  of the lowest-lying two-body bound states. For instance, the latter is also composed of an intraband contribution  $(M_{2b}^{-1})_{ij}^{\text{intra}} = \frac{2}{D} \sum_{\mathbf{k}} \partial_i \varepsilon_{n\mathbf{k}} \partial_j \varepsilon_{n\mathbf{k}} / (2\varepsilon_{n\mathbf{k}} - E_b)^3$  and an interband contribution  $(M_{2b}^{-1})_{ij}^{\text{inter}} = \frac{1}{D} \sum_{n\mathbf{k}} g_{ij}^{n\mathbf{k}} / (2\varepsilon_{n\mathbf{k}} - E_b) - \frac{1}{D} \sum_{n,m \neq n,\mathbf{k}} g_{ij}^{n\mathbf{k}} / (\varepsilon_{n\mathbf{k}} + \varepsilon_{m\mathbf{k}} - E_b)$ , where  $D = \sum_{n\mathbf{k}} 1/(2\varepsilon_{n\mathbf{k}} - E_b)^2$  [6].

In particular, we note that since the so-called geometric contribution  $(\xi_{2b}^2)_{ij}^{\text{inter}}$  is not due to the non-zero center-of-mass momentum  $\mathbf{q}$  of the pair, its physical origin differs from that of  $(M_{2b}^{-1})_{ij}^{\text{inter}}$ . In other words, while the

interband contributions to the superfluid density, low-energy collective modes, GL coherence length, and similar quantities are all directly linked to each other through the effective-mass tensor of the Cooper pairs [6, 14], and whose origin can be traced all the way back to  $(M_{2b}^{-1})_{ij}^{\text{inter}}$ , the localization tensor is not one of them. On the other hand, despite their difference in origin,  $(\xi_{2b}^2)_{ij}^{\text{inter}}$  does not receive any contribution from band touchings, which is similar to  $(M_{2b}^{-1})_{ij}^{\text{inter}}$ . Specifically, the first sum cancels the contributions from the second sum at the band touchings, i.e., whenever  $\varepsilon_{n\mathbf{k}} = \varepsilon_{m\mathbf{k}}$  for any  $n \neq m$ .

It is also important to emphasize that Eqs. (11) and (12) are exact for the lowest-lying  $\mathbf{q} = \mathbf{0}$  bound state under the assumptions of time-reversal symmetry and uniform pairing, where Eq. (11) is simply a sum over the well-known single-band expression [21]. In the case of an energetically-isolated flat band that is separated from the remaining bands with a finite band gap, they reduce to

$$(\xi_{2b}^2)_{ij} \rightarrow \frac{1}{N_c} \sum_{\mathbf{k}} g_{ij}^{f\mathbf{k}} \quad (13)$$

in the  $U/t \rightarrow 0$  limit, where  $g_{ij}^{f\mathbf{k}}$  is the quantum metric of the flat band, which is in agreement with a recent preprint [22]. Note that  $(M_{2b}^{-1})_{ij} \rightarrow \frac{U}{N} \sum_{\mathbf{k}} g_{ij}^{f\mathbf{k}}$  in the very same limit [3]. Furthermore, we also note that  $(\xi_0^2)_{ij} \rightarrow \frac{1}{8FN} \sum_{\mathbf{k}} g_{ij}^{f\mathbf{k}}$  for the zero-temperature coherence length and  $(\xi_{\text{GL}}^2)_{ij} \rightarrow \frac{1}{3FN} \sum_{\mathbf{k}} g_{ij}^{f\mathbf{k}}$  for the GL coherence length near the critical temperatures, i.e., for a dilute isolated flat-band superconductor when the particle filling  $F \rightarrow 0$  [14]. Next, we benchmark Eqs. (11) and (12) against an analogous tensor for the average size of Cooper pairs within the variational BCS mean-field theory, under the same assumptions.

#### IV. MEAN-FIELD BCS PROBLEM

Assuming time-reversal symmetry for the Bloch Hamiltonian and uniform pairing across the lattice sites, the BCS ground state can be written as [6]

$$|\text{BCS}\rangle = \prod_{n\mathbf{k}} (u_{n\mathbf{k}} + v_{n\mathbf{k}} c_{n\uparrow}^\dagger c_{n,-\mathbf{k},\downarrow}^\dagger) |0\rangle, \quad (14)$$

where  $u_{n\mathbf{k}} = \sqrt{\frac{1}{2} + \frac{\xi_{n\mathbf{k}}}{2E_{n\mathbf{k}}}}$  and  $v_{n\mathbf{k}} = \sqrt{\frac{1}{2} - \frac{\xi_{n\mathbf{k}}}{2E_{n\mathbf{k}}}}$  are the usual coherence factors. Here,  $\xi_{n\mathbf{k}} = \varepsilon_{n\mathbf{k}} - \mu$  is the energy measured relative to the chemical potential  $\mu$ , and  $E_{n\mathbf{k}} = \sqrt{\xi_{n\mathbf{k}}^2 + \Delta_0^2}$  is the quasiparticle dispersion. The BCS expectation value  $\Delta_{S_i} = U \langle c_{S_i\uparrow} c_{S_i\downarrow} \rangle$  is taken as  $\Delta_0$  for every sublattice site  $S$  within any unit cell  $i$ , representing the uniform BCS order parameter for pairing, i.e.,  $\Delta_0 \equiv \frac{1}{N} \sum_{S_i} \Delta_{S_i}$ , leading to  $\Delta_0 = \frac{U}{N} \sum_{n\mathbf{k}} \langle c_{n\uparrow} c_{n,-\mathbf{k},\downarrow} \rangle$ , which is assumed to be real without loss of generality. In the zero-temperature BCS-BEC crossover formalism [23, 24], it is sufficient to find  $\mu$  and  $\Delta_0$  from the

self-consistent solutions of the mean-field gap equation  $1 = \frac{U}{N} \sum_{n\mathbf{k}} 1/(2E_{n\mathbf{k}})$  and the mean-field number equation  $F = 1 - \frac{1}{N} \sum_{n\mathbf{k}} \xi_{n\mathbf{k}}/E_{n\mathbf{k}}$ , where the particle filling  $0 \leq F = \mathcal{N}/N \leq 2$  corresponds to the total number of particles per lattice site.

Motivated by the pair-correlation function with opposite spins, the wave function for the Cooper pairs can be written as [23–26]

$$\Phi(r_1, r_2) = \langle \text{BCS} | \psi_\uparrow^\dagger(r_1) \psi_\downarrow^\dagger(r_2) | \text{BCS} \rangle, \quad (15)$$

where the operator  $\psi_\sigma^\dagger(r) = \sum_{n\mathbf{k}} \phi_{n\mathbf{k}\sigma}^*(r) c_{n\mathbf{k}\sigma}^\dagger$  creates a spin- $\sigma$  fermion at position  $r$  and  $\phi_{n\mathbf{k}\sigma}(r)$  is the Bloch wave function. Inserting  $\langle \text{BCS} | c_{n\mathbf{k}\uparrow}^\dagger c_{m\mathbf{k}'\downarrow}^\dagger | \text{BCS} \rangle = \delta_{nm} \delta_{\mathbf{k}, -\mathbf{k}'} u_{n\mathbf{k}} v_{n\mathbf{k}} n_{\mathbf{k}\uparrow}^*(r_1) n_{-\mathbf{k},\downarrow}^*(r_2)$ . Thus, the role of  $\alpha_{n\mathbf{k}}^0$  in the two-body wave function  $\Psi_0(r_1, r_2)$  is effectively played by  $\frac{1}{\sqrt{A_{Cp}}} u_{n\mathbf{k}} v_{n\mathbf{k}}$  in  $\Phi(r_1, r_2)$ , where  $A_{Cp} = \sum_{n\mathbf{k}} u_{n\mathbf{k}}^2 v_{n\mathbf{k}}^2 = \sum_{n\mathbf{k}} \Delta_0^2 / (4E_{n\mathbf{k}}^2)$  is the normalization factor. Note that this observation is consistent with the number of condensed pairs, which is determined by  $\sum_{nSS'\mathbf{k}} |u_{n\mathbf{k}} v_{n\mathbf{k}} n_{S\mathbf{k}} n_{S'\mathbf{k}}^*|^2 = A_{Cp}$ , i.e., the mean-field expression for the filling of condensed particles is  $F_c = \frac{1}{N} \sum_{n\mathbf{k}} \Delta_0^2 / (2E_{n\mathbf{k}}^2)$  [6, 27].

Analogous to the localization tensor introduced in Eq. (7), the average size of Cooper pairs can be characterized using a related tensor

$$(\xi_{Cp}^2)_{ij} = \sum_{r_1 r_2} r_i r_j |\Phi(r_1, r_2)|^2, \quad (16)$$

where  $\mathbf{r} = r_1 - r_2$  is the relative position between two particles, and  $r_i$  is its  $i$ -component. Having continuum systems in mind, the pair size is typically defined as the trace of the localization tensor in the BCS-BEC crossover theories [23–26]. However, here we extend this concept to its tensorial form to highlight its deep connection to the quantum-metric tensor in multiband Hubbard models. Following a similar approach as in Eq. (8), we find that  $(\xi_{Cp}^2)_{ij} = \frac{1}{A_{Cp}} \sum_{nmSS'\mathbf{k}} \partial_i (u_{n\mathbf{k}} v_{n\mathbf{k}} n_{S\mathbf{k}} n_{S'\mathbf{k}}^*) \partial_j (u_{m\mathbf{k}} v_{m\mathbf{k}} m_{S\mathbf{k}}^* m_{S'\mathbf{k}})$ . This expression can also be separated into intra-band and interband contributions as  $(\xi_{Cp}^2)_{ij} = (\xi_{Cp}^2)_{ij}^{\text{intra}} + (\xi_{Cp}^2)_{ij}^{\text{inter}}$ , where

$$(\xi_{Cp}^2)_{ij}^{\text{intra}} = \frac{\sum_{n\mathbf{k}} \partial_i \varepsilon_{n\mathbf{k}} \partial_j \varepsilon_{n\mathbf{k}} \frac{\xi_{n\mathbf{k}}^2}{E_{n\mathbf{k}}^6}}{\sum_{n\mathbf{k}} \frac{1}{E_{n\mathbf{k}}^2}}, \quad (17)$$

$$(\xi_{Cp}^2)_{ij}^{\text{inter}} = \frac{\sum_{n\mathbf{k}} \frac{g_{ij}^{n\mathbf{k}}}{E_{n\mathbf{k}}^2} - \sum_{n, m \neq n, \mathbf{k}} \frac{g_{ij}^{n\mathbf{k}}}{E_{n\mathbf{k}} E_{m\mathbf{k}}}}{\sum_{n\mathbf{k}} \frac{1}{E_{n\mathbf{k}}^2}}. \quad (18)$$

Note that Eq. (17) is simply a sum over the well-known single-band expression [23, 24]. In the context of cold Fermi gases, this latter length scale was shown to qualitatively agree with the pair size extracted from

radio-frequency-spectrum measurements across the BCS-BEC crossover [25]. Furthermore, similarly to  $(\xi_{2b}^2)_{ij}^{\text{inter}}$ ,  $(\xi_{Cp}^2)_{ij}^{\text{inter}}$  also receives no contribution from band touchings, i.e., the first sum cancels those touching contributions from the second sum whenever  $\varepsilon_{n\mathbf{k}} = \varepsilon_{m\mathbf{k}}$  for any  $n \neq m$ . It is also reassuring to see that Eqs. (17) and (18) reproduce Eqs. (11) and (12), respectively, in the dilute limit  $F \ll 1$  where  $\mu \rightarrow E_b/2 < 0$  and  $\xi_{n\mathbf{k}} \gg \Delta_0$  for every state in the BZ. This is typically the case in the BEC limit when  $U/t \gg 1$ , but not when moving away from it towards the BCS regime of dispersive bands.

The pair size is a meaningful observable, representing the characteristic length scale associated with the pair-correlation function. Its physical significance is well-established in the BCS-BEC crossover literature [23–26]. For instance, in the continuum limit, the pair size aligns (up to a factor of order unity) with the phase coherence length in the BCS regime, while it precisely matches the size of two-body bound states in the BEC regime. This duality underscores its utility in capturing pair correlations across the crossover.

## V. NUMERICAL ILLUSTRATION

As a numerical illustration of our analytical expressions, we study the pyrochlore lattice, which is obtained by constructing the line graph of the diamond lattice, featuring two degenerate flat bands in three dimensions. Its crystal structure is a face-centered-cubic Bravais lattice with a four-point basis, resulting in a truncated-octahedron-shaped BZ. Recent demonstrations of flat bands and superconductivity in materials such as the pyrochlore metal  $\text{CaNi}_2$  [28] and the pyrochlore superconductor  $\text{CeRu}_2$  [29] highlight the growing relevance of this model in understanding emergent quantum phenomena. Its Bloch Hamiltonian is determined by  $h_{S\mathbf{S}\mathbf{k}}^\sigma = 0$ ,  $h_{AB\mathbf{k}}^\sigma = -2\bar{t} \cos\left(\frac{k_y+k_z}{4}a\right)$ ,  $h_{AC\mathbf{k}}^\sigma = -2\bar{t} \cos\left(\frac{k_x+k_z}{4}a\right)$ ,  $h_{AD\mathbf{k}}^\sigma = -2\bar{t} \cos\left(\frac{k_x+k_y}{4}a\right)$ ,  $h_{BC\mathbf{k}}^\sigma = -2\bar{t} \cos\left(\frac{k_x-k_y}{4}a\right)$ ,  $h_{BD\mathbf{k}}^\sigma = -2\bar{t} \cos\left(\frac{k_x-k_z}{4}a\right)$  and  $h_{CD\mathbf{k}}^\sigma = -2\bar{t} \cos\left(\frac{k_y-k_z}{4}a\right)$ , where  $\bar{t}$  is the tight-binding hopping parameter between nearest-neighbor sites and  $a$  is the side-length of the conventional simple-cubic cell [6, 14]. The resulting Bloch spectrum comprises two dispersive bands given by  $\varepsilon_{1\mathbf{k}\sigma} = -2\bar{t}(1 + \sqrt{1 + \gamma_{\mathbf{k}}})$  and  $\varepsilon_{2\mathbf{k}\sigma} = -2\bar{t}(1 - \sqrt{1 + \gamma_{\mathbf{k}}})$ , where  $\gamma_{\mathbf{k}} = \cos(k_x a/2) \cos(k_y a/2) + \cos(k_y a/2) \cos(k_z a/2) + \cos(k_x a/2) \cos(k_z a/2)$ , as well as two degenerate flat bands given by  $\varepsilon_{3\mathbf{k}\sigma} = \varepsilon_{4\mathbf{k}\sigma} = 2\bar{t}$ . To position these flat bands at the bottom of the spectrum, we set  $\bar{t} \rightarrow -t$  and choose  $t > 0$  as the unit of energy. Note that  $\varepsilon_{2\mathbf{k}\sigma}$  touches the flat bands at  $\mathbf{k} = \mathbf{0}$ .

In our previous work on the pyrochlore lattice [6], we explored various connections between the superfluid-weight tensor and the effective-mass tensor of the lowest-lying two-body branch at zero temperature, the kinetic coefficient in the GL theory near the critical temperature, and the velocity of low-energy Goldstone modes

at zero temperature [6]. In addition, we analyzed the GL coherence length near the critical temperature and compared it with the zero-temperature coherence length, both of which are tied to the effective-mass tensor of Cooper pairs [14]. While these studies also focus on the pyrochlore lattice, the topics they address are distinct from the current paper, with no overlap.

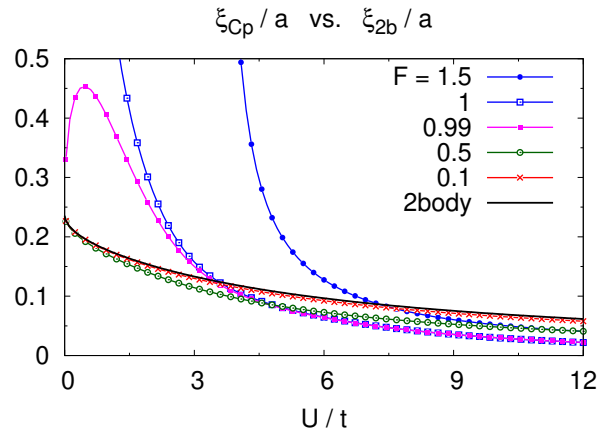


FIG. 1. While the average size of Cooper pairs diverges in the BCS regime  $1 < F < 2$  of dispersive bands as  $\Delta_0/t \rightarrow 0$  in the  $U/t \rightarrow 0$  limit, it approaches the size of the lowest-lying two-body bound state in the dilute flat-band regime for any  $U \neq 0$ , as the particle filling  $F \rightarrow 0$ .

Since the pyrochlore-Hubbard model exhibits both time-reversal symmetry and uniform-pairing condition [6, 14], we can directly apply Eqs. (11) and (12) to the two-body problem and Eqs. (17) and (18) to the many-body problem. The results are shown in Fig. 1, where  $(\xi_{2b}^2)_{ij} = \xi_{2b}^2 \delta_{ij}$  and  $(\xi_{Cp}^2)_{ij} = \xi_{Cp}^2 \delta_{ij}$  as a consequence of uniform pairing. In the absence of interactions, when  $U = 0$ ,  $-2t < \mu < 6t$  lies within the dispersive bands when  $1 < F < 2$ . Here,  $\mu = 2t$  corresponds to  $F = 1.5$  and  $\mu \rightarrow -2t$  from above corresponds to a half-filled lattice with  $F \rightarrow 1$  from above. Note that  $\mu = -2t$  coincides with the degenerate flat bands when  $0 < F < 1$ . Thus, Fig. 1 shows that the pair size  $\xi_{Cp}$  diverges in the BCS regime  $1 < F < 2$  of dispersive bands as  $\Delta_0/t \rightarrow 0$  in the  $U/t \rightarrow 0$  limit, which is consistent with the BCS behavior in the usual BCS-BEC crossover problem [23, 24]. In contrast,  $\xi_{Cp}$  remains finite and relatively small for the flat-band regime  $0 < F < 1$  as  $\Delta_0/t \rightarrow 0$  in the  $U/t \rightarrow 0$  limit, and does not diverge. The striking difference between the  $U/t \rightarrow 0$  limit of the BCS regime of dispersive bands and the flat-band regime is in accordance with the modern theory of insulating states: the localization tensor diverges in the thermodynamic limit in any metal, while it remains finite in any insulator [1]. Due to the presence of compact localized states in the non-interacting spectrum, the flat-band regime behaves similarly to an insulating state. Furthermore, Fig. 1 shows that  $\xi_{Cp}$  approaches the size  $\xi_{2b}$  of the lowest-lying two-body bound

state for all  $U \neq 0$  in the dilute limit as  $F \rightarrow 0$ . In this case, it can be shown that  $\xi_{Cp} \rightarrow \xi_{2b}$  term by term for all  $U \neq 0$ . In particular, when  $U/t \rightarrow 0$ , we find  $\xi_{2b}^{\text{intra}} \rightarrow 0$  and  $(\xi_{2b}^{\text{inter}})^2 \rightarrow \frac{1}{N_c} \sum'_{m \notin f, \mathbf{k}} g_{xx}^{fm\mathbf{k}} \approx 0.056a^2$ , where  $f = \{3, 4\}$  refers to the flat bands and  $m = \{1, 2\}$  refers to the dispersive bands, and the prime sum excludes the band touchings. Thus, we expect  $\xi_{2b} \approx 0.24a$  in the  $U/t \rightarrow 0$  limit, which is consistent with Fig. 1. Note that the shortest distance between lattice sites is approximately  $a/\sqrt{8} \approx 0.35a$  for the pyrochlore lattice.

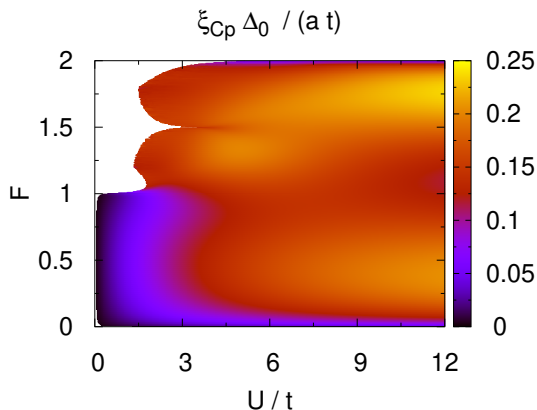


FIG. 2. The average size of Cooper pairs scales as  $t/\Delta_0$  in most of the parameter space, except for the case of flat-band superconductivity in the low- $U/t$  regime. Since our numerics become unreliable in the limit  $\Delta_0/t \rightarrow 0$ , we present only the data with  $\Delta_0/t > 0.01$ , which reveals the underlying single-particle density of states at the periphery of the white region, i.e., in the BCS regime of dispersive bands when  $1 < F < 2$  [6].

In Fig. 2, we present a color map of  $\xi_{Cp}$  as a function of  $F$  and  $U/t$ . This map shows that  $\xi_{Cp}$  scales as  $t/\Delta_0$  over most of the parameter space, which is in perfect agreement with the BCS result, except in the flat-band regime at low  $U/t$ . In the latter regime,  $\xi_{Cp}$  is governed solely by the quantum geometry of the Bloch states. A similar scaling behavior has recently been reported for a related correlation length in the context of the sawtooth lattice [30]. Furthermore, Fig. 2 bears resemblance to results on zero-temperature coherence length, which also scales as  $t/\Delta_0$  in most of the parameter space [14]. However, while coherence length and  $\xi_{Cp}$  differ only by a factor of order unity around  $F = 0.5$ , i.e., around the half-filled flat-band regime, coherence length becomes much larger than  $\xi_{Cp} \rightarrow \xi_{2b}$  in the dilute flat-band regime as  $F \rightarrow 0$ . For instance, the coherence length  $\xi_0^2 \rightarrow \frac{1}{4FN} \sum'_{m \notin f, \mathbf{k}} g_{xx}^{fm\mathbf{k}}$  diverges as  $F \rightarrow 0$  in the  $U/t \rightarrow 0$  limit [14]. This finding is consistent with the BEC behavior in the usual BCS-BEC crossover problem [24, 31].

## VI. CONCLUSION

In summary, by considering a multiband Hubbard model that exhibits time-reversal symmetry and uniform pairing in the lattice, we analyzed how the quantum geometry of the Bloch states affects: (i) the size of lowest-lying two-body bound state in vacuum through an exact calculation of the localization tensor, and (ii) the average size of Cooper pairs through a related tensor within the mean-field BCS-BEC crossover theory at zero temperature. Our primary finding is that, in contrast to the BCS regime of dispersive bands, where the pair size is known to diverge as  $t/\Delta_0$  when the order parameter  $\Delta_0/t \rightarrow 0$  in the weakly-interacting  $U/t \rightarrow 0$  limit, it remains finite and relatively small in the flat-band regime under the very same conditions, perfectly matching the exact two-body result in the dilute limit.

The pair size bears resemblance to recent results on the zero-temperature coherence length, which also scales as  $t/\Delta_0$  in most of the parameter space [14]. However, in the flat-band regime, the pair size remains finite and relatively small, being governed solely by the quantum metric in the dilute limit. Thus, we emphasized that the pair size and coherence length are distinct physical quantities, particularly in the dilute limit. Furthermore, as revealed in this paper through an exact calculation of the two-body problem, their quantum-geometric origins in a multiband Hubbard model are also distinct. Similar to superfluid density, low-energy collective modes, and the GL coherence length, while the zero-temperature coherence length is directly related to the motion of Cooper pairs through the inverse effective-mass tensor [6, 14], the pair size is not. In other words, the quantum-geometric origin of the pair size does not stem from the non-zero center-of-mass momentum of the pair, which distinguishes it from previous findings in this context. Thus, the quantum-geometric effects that influence these quantities operate in fundamentally different ways.

## ACKNOWLEDGMENTS

The author acknowledges funding from US Air Force Office of Scientific Research (AFOSR) Grant No. FA8655-24-1-7391.

### Appendix A: An unphysical length scale

Motivated by recent literature on spin-orbit-coupled Fermi gases [26], we propose an alternative, yet ultimately unsuccessful, approach to the wave function of Cooper pairs. For this purpose, the BCS ground state, given by Eq. (14), can equivalently be written as  $|\text{BCS}\rangle = (\prod_{n\mathbf{k}} u_{n\mathbf{k}}) e^{\sum_{n\mathbf{k}} \frac{v_{n\mathbf{k}}}{u_{n\mathbf{k}}} c_{n\mathbf{k}\uparrow}^\dagger c_{n,-\mathbf{k},\downarrow}^\dagger} |0\rangle$ . This reformulation sug-

gests that the state

$$|\Phi_p\rangle = \frac{1}{\sqrt{A_p}} \sum_{n\mathbf{k}} \frac{v_{n\mathbf{k}}}{u_{n\mathbf{k}}} c_{n\mathbf{k}\uparrow}^\dagger c_{n,-\mathbf{k},\downarrow}^\dagger |0\rangle \quad (\text{A1})$$

may represent Cooper pairs in a many-body setting, where  $A_p = \sum_{n\mathbf{k}} v_{n\mathbf{k}}^2 / u_{n\mathbf{k}}^2 = \sum_{n\mathbf{k}} (E_{n\mathbf{k}} - \xi_{n\mathbf{k}})^2 / \Delta_0^2$  is the normalization factor. Thus, the role of  $\alpha_{n\mathbf{k}}^0$  in the two-body ansatz  $|\Psi_0\rangle$  is effectively played by  $\frac{1}{\sqrt{A_p}} \frac{v_{n\mathbf{k}}}{u_{n\mathbf{k}}}$  in  $|\Phi_p\rangle$ . Then, following a similar approach as in Eq. (8), we find that  $(\xi_p^2)_{ij} = \frac{1}{A_p} \sum_{nmS'S'\mathbf{k}} \partial_i \left( \frac{v_{n\mathbf{k}}}{u_{n\mathbf{k}}} n_{S\mathbf{k}} n_{S'\mathbf{k}}^* \right) \partial_j \left( \frac{v_{m\mathbf{k}}}{u_{m\mathbf{k}}} m_{S\mathbf{k}}^* m_{S'\mathbf{k}} \right)$ , and separate it into intraband and interband contributions as  $(\xi_p^2)_{ij} = (\xi_p^2)_{ij}^{\text{intra}} + (\xi_p^2)_{ij}^{\text{inter}}$ , where

$$(\xi_p^2)_{ij}^{\text{intra}} = \frac{\sum_{n\mathbf{k}} \partial_i \varepsilon_{n\mathbf{k}} \partial_j \varepsilon_{n\mathbf{k}} \left( 1 - \frac{\xi_{n\mathbf{k}}}{E_{n\mathbf{k}}} \right)^2}{\sum_{n\mathbf{k}} (E_{n\mathbf{k}} - \xi_{n\mathbf{k}})^2}, \quad (\text{A2})$$

$$(\xi_p^2)_{ij}^{\text{inter}} = \frac{\sum_{n\mathbf{k}} (E_{n\mathbf{k}} - \xi_{n\mathbf{k}})^2 g_{ij}^{n\mathbf{k}}}{\sum_{n\mathbf{k}} (E_{n\mathbf{k}} - \xi_{n\mathbf{k}})^2} - \frac{\sum_{n,m \neq n,\mathbf{k}} (E_{n\mathbf{k}} - \xi_{n\mathbf{k}})(E_{m\mathbf{k}} - \xi_{m\mathbf{k}}) g_{ij}^{nm\mathbf{k}}}{\sum_{n\mathbf{k}} (E_{n\mathbf{k}} - \xi_{n\mathbf{k}})^2}. \quad (\text{A3})$$

Note that, similarly to  $(\xi_{2b}^2)_{ij}^{\text{inter}}$  and  $(\xi_{Cp}^2)_{ij}^{\text{inter}}$ ,  $(\xi_p^2)_{ij}^{\text{inter}}$  also receives no contribution from band touchings.

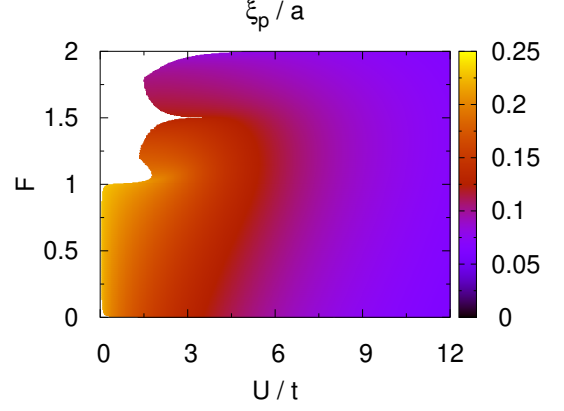


FIG. 3. In the low- $U/t$  regime, while the length scale  $\xi_p$  qualitatively reproduces the correct results for the average size of Cooper pairs in the flat-band regime, e.g., it coincides perfectly with the size of the lowest-lying two-body bound state in the dilute flat-band limit as  $F \rightarrow 0$ , it gives unphysical results for the BCS regime of dispersive bands when  $1 < F < 2$ , as it saturates in that range even though  $\Delta_0/t \rightarrow 0$ .

In Fig. 3, we present a color map of  $\xi_p$  for the pyrochlore lattice, demonstrating that  $\xi_p$  does not diverge in the BCS regime  $U/t \rightarrow 0$ , even as  $\Delta_0/t \rightarrow 0$  for the dispersive bands when  $1 < F < 2$ . Since this behavior contrasts sharply with physical expectations [23, 24], we conclude that  $\xi_p$  does not represent a physically meaningful observable length scale. On the other hand,  $\xi_p$  coincides perfectly with  $\xi_{2b}$  and  $\xi_{Cp}$  for any  $U \neq 0$  in the dilute flat-band limit when  $F \rightarrow 0$ . In this particular case, assuming  $\xi_{n\mathbf{k}} \gg \Delta_0$  for every state in the BZ, it can be shown analytically that Eqs. (A2) and (A3) are identical to Eqs. (17) and (18), respectively, where  $v_{n\mathbf{k}}/u_{n\mathbf{k}} \approx v_{n\mathbf{k}}/u_{n\mathbf{k}} \approx \Delta_0/(2\xi_{n\mathbf{k}})$  at the leading order.

- 
- [1] R. Resta, The insulating state of matter: a geometrical theory, *The European Physical Journal B* **79**, 121 (2011).
- [2] P. Törmä, Essay: Where can quantum geometry lead us?, *Phys. Rev. Lett.* **131**, 240001 (2023).
- [3] P. Törmä, S. Peotta, and B. A. Bernevig, Superconductivity, superfluidity and quantum geometry in twisted multilayer systems, *Nature Reviews Physics* **4**, 528 (2022).
- [4] K.-E. Huhtinen, J. Herzog-Arbeitman, A. Chew, B. A. Bernevig, and P. Törmä, Revisiting flat band superconductivity: Dependence on minimal quantum metric and band touchings, *Phys. Rev. B* **106**, 014518 (2022).
- [5] J. Herzog-Arbeitman, A. Chew, K.-E. Huhtinen, P. Törmä, and B. A. Bernevig, Many-body superconductivity in topological flat bands (2022), [arXiv:2209.00007](https://arxiv.org/abs/2209.00007).
- [6] M. Iskin, Cooper pairing, flat-band superconductivity, and quantum geometry in the pyrochlore-Hubbard model, *Phys. Rev. B* **109**, 174508 (2024).
- [7] A. Daido, T. Kitamura, and Y. Yanase, Quantum geometry encoded to pair potentials, (2023), [arXiv:2310.15558](https://arxiv.org/abs/2310.15558).
- [8] M. Iskin, Extracting quantum-geometric effects from Ginzburg-Landau theory in a multiband Hubbard model, *Phys. Rev. B* **107**, 224505 (2023).
- [9] S. A. Chen and K. T. Law, Ginzburg-Landau theory of flat-band superconductors with quantum metric, *Phys. Rev. Lett.* **132**, 026002 (2024).
- [10] N. Verma, D. Guerci, and R. Queiroz, Geometric stiffness in interlayer exciton condensates, *Phys. Rev. Lett.* **132**, 236001 (2024).
- [11] G. Jiang and Y. Barlas, Pair density waves from local band geometry, *Phys. Rev. Lett.* **131**, 016002 (2023).
- [12] G. Jiang and Y. Barlas, Geometric superfluid weight of composite bands in multiorbital superconductors, *Phys. Rev. B* **109**, 214518 (2024).
- [13] T. Kitamura, A. Daido, and Y. Yanase, Spin-triplet superconductivity from quantum-geometry-induced ferromagnetic fluctuation, *Phys. Rev. Lett.* **132**, 036001 (2024).
- [14] M. Iskin, Coherence length and quantum geometry in a dilute flat-band superconductor, *Phys. Rev. B* **110**,

- 144505 (2024).
- [15] Z. Han, J. Herzog-Arbeitman, B. A. Bernevig, and S. A. Kivelson, Quantum geometric nesting and solvable model flat-band systems, arXiv preprint arXiv:2401.04163 (2024).
- [16] Y.-J. Hu and W. Huang, Quantum geometric superfluid weight in multiband superconductors: A microscopic interpretation, arXiv preprint arXiv:2409.12254 (2024).
- [17] M. Iskin, Quantum-metric contribution to the pair mass in spin-orbit-coupled Fermi superfluids, *Phys. Rev. A* **97**, 033625 (2018).
- [18] M. Iskin, Two-body problem in a multiband lattice and the role of quantum geometry, *Phys. Rev. A* **103**, 053311 (2021).
- [19] N. W. Ashcroft and N. D. Mermin, *Solid State Physics* (Holt, Rinehart and Winston, New York, 1976) appendix I.
- [20] For instance, using the Green's theorem for periodic functions [19], it can be written as  $(\xi_{2b}^2)_{ij} = -\sum_{nmn'm'S'S'\mathbf{k}} \alpha_{nm\mathbf{k}}^{\mathbf{q}} n_{S,\mathbf{k}+\frac{\mathbf{q}}{2},\uparrow} m_{S',-\mathbf{k}+\frac{\mathbf{q}}{2},\downarrow} \partial_i \partial_j (\alpha_{n'm'\mathbf{k}}^{\mathbf{q}} n'_{S,\mathbf{k}+\frac{\mathbf{q}}{2},\uparrow} m'_{S',-\mathbf{k}+\frac{\mathbf{q}}{2},\downarrow})^*$ .
- [21] P.-G. de Gennes, *Superconductivity of Metals and Alloys* (W.A. Benjamin, Inc., New York, 1966) chapter 4.
- [22] X. Ying and K. T. Law, Flat band excitons and quantum metric, arXiv preprint arXiv:2407.00325 (2024).
- [23] F. Pistolesi and G. C. Strinati, Evolution from BCS superconductivity to Bose condensation: Role of the parameter  $k_f \xi$ , *Phys. Rev. B* **49**, 6356 (1994).
- [24] J. R. Engelbrecht, M. Randeria, and C. A. R. Sáde Melo, BCS to Bose crossover: Broken-symmetry state, *Phys. Rev. B* **55**, 15153 (1997).
- [25] C. H. Schunck, Y.-i. Shin, A. Schirotzek, and W. Ketterle, Determination of the fermion pair size in a resonantly interacting superfluid, *Nature* **454**, 739 (2008).
- [26] Y. Yi-Xiang, J. Ye, and W.-M. Liu, Coherence lengths in attractively interacting Fermi gases with spin-orbit coupling, *Phys. Rev. A* **90**, 053603 (2014).
- [27] A. J. Leggett, *Quantum Liquids: Bose Condensation and Cooper Pairing in Condensed-Matter Systems* (Oxford University Press, Oxford, UK, 2006).
- [28] J. P. Wakefield, M. Kang, P. M. Neves, D. Oh, S. Fang, R. McTigue, S. Frank Zhao, T. N. Lamichhane, A. Chen, S. Lee, *et al.*, Three-dimensional flat bands in pyrochlore metal CaNi<sub>2</sub>, *Nature* **623**, 301 (2023).
- [29] J. Huang, C. Setty, L. Deng, J.-Y. You, H. Liu, S. Shao, J. S. Oh, Y. Guo, Y. Zhang, Z. Yue, *et al.*, Observation of flat bands and Dirac cones in a pyrochlore lattice superconductor, (2023), arXiv:2304.09066.
- [30] M. Thumin and G. Bouzerar, Correlation functions and characteristic lengthscales in flat band superconductors, arXiv preprint arXiv:2405.06215 (2024).
- [31] F. Pistolesi and G. C. Strinati, Evolution from BCS superconductivity to Bose condensation: Calculation of the zero-temperature phase coherence length, *Phys. Rev. B* **53**, 15168 (1996).